Journal of Advanced Research in Fluid Mechanics and Thermal Sciences

Journal homepage:
https://semarakilmu.com.my/journals/index.php/fluid_mechanics_thermal_sciences/index
ISSN: 2811-3950

Modeling and Simulation of PMSG Wind Energy Conversion System Using Active Disturbance Rejection Control

Safwan Sadeq[1], Mark Ovinis[1,*], Saravanan Karuppanan[1]

[1] Department of Mechanical Engineering, Universiti Teknologi PETRONAS Malaysia, 31750 Seri Iskandar, Perak, Malaysia

ARTICLE INFO

Article history:
Received 1 November 2021
Received in revised form 27 December 2021
Accepted 30 December 2021
Available online 2 February 2022

Keywords:
Active Disturbance Rejection Controller (ADRC); Extended state observer ESO; Permanent Magnet Synchronous Generator (PMSG)

ABSTRACT

Electrical power generated from wind turbines inherently fluctuates due to changing wind speeds. Without proper control, disturbances such as changing wind speeds can degrade the power quality factor and robustness of the electrical grid. To ensure good power quality factor, high performance and robustness of the grid against internal and external disturbances, the use of Active Disturbance Rejection Control with an extended state observer ESO for a PMSG Wind Energy Conversion System is investigated. The system has been simulated in MATLAB/Simulink at various wind speeds. The obtained simulation results indicate that the controller maintains constant DC voltage at the interface of the generator-side converter and grid-side converters and achieves maximum power. The results also show that the system performance has good stability, precision and rejection of internal disturbances, with an overall system efficiency of 98.65%.

1. Introduction

Lately, the demand for electrical power is increasing exponentially. Most of conventional electrical power generators run on fossil fuels, which is financially costly–and harmful to the environment. So, the adoption of sustainable and green energy-based technologies such as solar energy and wind energy is gaining popularity. Other green energy-based resources currently being explored include fuel cells, geothermal energy, and ocean energy [1]. The increasing cost of fossil fuel compared to the reducing cost of green energy-based power is one of the drivers for the current energy shift from fossil fuel-based energy resources to green energy-based resources [2].

Recently, there is an increase in the number of homes and organizations introducing small wind turbines to reduce utility bills and carbon dioxide productions. In the event extra power is produced, additional power can be sold to the national grid. The wind energy market in developed regions is on the rise, with rapid deployment renewable energy technologies. Globally, there is an enormous amount of small-scale wind turbines that are installed with an installed capacity of around 7.42 GW as of 2020 [3]. Wind based energy is intermittent and discontinuous in nature, therefore requires

* *Corresponding author.*
E-mail address: mark_ovinis@utp.edu.my

https://doi.org/10.37934/arfmts.92.1.105122

specialized control. So far, various topologies and configurations of wind energy-based systems have been presented. A general configuration for a wind energy conversion system (WECS) is shown in Figure 1, with flexibility in generator and power converter typology. The current existing generators on the market are predominantly DC generators namely 3-phase synchronous generator (SG), permanent magnet synchronous generator (PMSG) and the doubly fed induction generator (DFIG). With the PMSG and DFIG typologies attracting more attention among developers and researchers due to their advanced power electronics technologies conducted by Gidwani [4]. The power converter options are single unit of 3-phase inverter (only if the generator is DC), a cascade of rectifier-fed dc-dc converter or a 3-phase inverter. For dc-dc converters, non-inverting buck-boost converters are also getting popular, because of the freedom it provides to track power over a wider input voltage range. A detailed block diagram for the wind energy system being investigated at present is shown in Figure 2. This system Configuration is suitable for regions with low wind speeds.

Fig. 1. General configuration of a wind energy conversion system

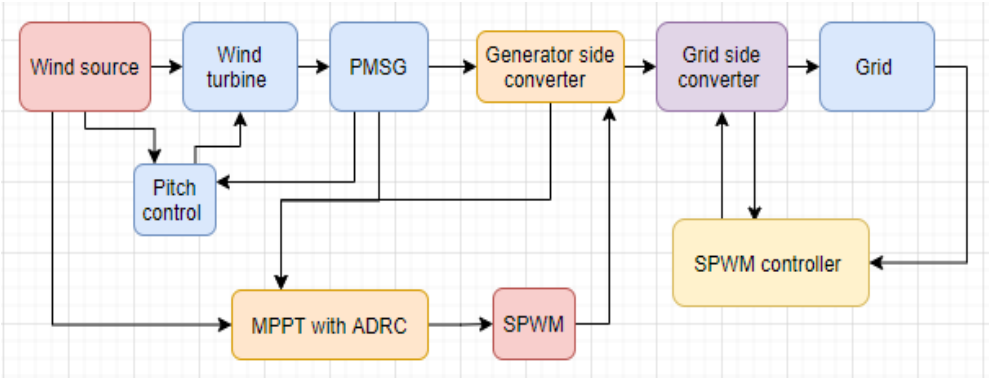

Fig. 2. System Block Diagram

Wind turbines operating at low wind speeds are required to greatly improve the operational performance. A study by Jamil *et al.,* [5] shows that modified three blade wind turbines with bumpy blade edges can perform better in low wind speed environments than turbines with smooth blade edges. However, Pichitkul *et al.,* [6] proposed a wind turbine design that operate over a wider range of wind speeds. This research work focuses on regions with low wind speeds such as Malaysia with an annual wind speed of less than 4 m/s [7]. However, the wind doesn't blow consistently throughout Malaysia and the wind speed changes based on month and region. Malaysia has two weather seasons namely southwest monsoon (May to September) and northeast monsoon (November to March). Wind speeds over the southwest monsoon are often below 7 m/s, but during the northeast monsoon, wind speeds can reach up to 15 m/s, particularly in the east coast of Malaysian Peninsula. However, Malaysia in general experiences low wind speeds. In this case study, the PMSG is used as the generator, followed by a rectifier, boost converter and 3-phase inverter. The rectifier is based on general purpose diodes, which are low frequency switching devices. Since the PMSG is driven at low rotational speeds, the resulting generator output voltage is of low frequency. This low-frequency output voltage can easily be rectified by the bridge rectifier. To maximize energy recovery, pitch control based on MPPT control optimizes the generator speed, The MPPT extracts the maximum

possible power and feeds it to the load via the boost converter, which steps up the voltage to the required magnitude.

In high wind regions where wind energy systems can be directly connected to the grid, doubly fed induction generators (DFIGs) dominate the field of large-scale wind-power generation, DFIG based systems have complex control due to various units within the system, resulting in power controllability issues in case of grid faults. These issues may compromise the reliability performance of the generator and make it hard to meet grid requirements conducted by Ma [8]. However, replacing the DFIG with the PMSG resolves several control issues. The biggest advantage is perhaps the decoupling of the controlling action to a large extent. In the case of DFIG, a complex controller is required for its smooth operation to synchronize with the grid. As the grid becomes weak, the robustness and tracking accuracy of the DFIG cannot be guaranteed and its control system becomes unstable but, replacing it with the PMSG eliminates the control effort requirement in the generator unit. However, in turbine pitch control, MPPT and boost converter and inverter (conversion from DC to AC) control effort is a necessity. Generally, all control actions are independent from one another, except the sharing of some error signals. The output voltage of a PMSG depends on its angular speed. This dependence can easily be avoided by using an appropriate interfacing converter with a suitable controller. Typically, PID control is widely used in most current PMSG implementations. PID control is the basic building block for Pitch control, MPPT control and inverter control. One of the advantages of PI controllers is that they are easy to implement, but there are four significant gaps with PID regulation namely error computation, noise degradation in the derivative control, oversimplification, and loss of performance in the control law in the form of a linear weighted sum. Although PID control can mitigate several issues, their performance to reject noise and disturbances is not satisfactory which was proposed by Han,[9]. The use of an active disturbance rejection controller is investigated in this paper in order to overcome the limitations of PID control. Additionally, if a WECS is linked to the grid, grid disturbances such as voltage dips can severely affect the performance of the PID controller. Previously, when such disturbances occurred, grid-connected wind turbine energy systems would have to be disconnected from the grid to protect system from being damaged [10]. The boost converter is the heart of the power conditioning unit for the WECS, when an MPPT extracts maximum possible power for the wind source the boost converter increases the output voltage to the load to required magnitude in proportion to the MPPT maximum power point which conducted by Illindala [11]. Good system performance can be ensured when the performance of the boost converter is robust to disturbances. The converter controller should actively reject internal or external disturbances. It must not only track the delivery of set-point power, but it must also reject any undesired input. Considering these constraints, an active disturbance rejection controller (ADRC) was selected due to its strong robustness and disturbance rejection, excellent performance, simple design and its convenience compared to the PID controller. The ADRC the advantages of the ADRC controller include fast response, robustness, and adaptability.

Due to wind speed variations, electrical power generated by a wind turbine fluctuates, when connected to the electrical grid this affects the power quality and robustness of the grid. To ensure good power factor regulation with high performance and robustness of the grid against the internal and the external disturbances, the use of Active Disturbance Rejection Control controller with an extended state observer ESO for a PMSG Wind Energy Conversion System is investigated.

Huang and Xue, stated that the core concept of the ADRC is based on the use an ESO for real-time estimation of internal and external disturbances [12]. The estimated disturbances are actively rejected without loading the controller. Thus, the only job of the controller remains that of tracking the references and system dynamics. The paper presents a simulation of PMSG wind energy conversion system using active disturbance rejection control. Obtained simulation results indicate

the controller maintains constant DC voltage at the interface of the generator-side converter and grid-side converters and achieves maximum power. The results also show that the system performance has good stability, precision and rejection of internal disturbances.

2. Literature Review

Three types of generators primarily used in wind conversion systems are the squirrel cage induction generator (SCIG), double-fed induction generator (DFIG) and the Permanent Magnet Synchronous Generator (PMSG) proposed by Elnaggar *et al.,* [13]. The PMSG can generate power at low speeds, even without a gearbox because of the higher number of poles. Figure 2 represent the configuration of a PMSG-based wind energy system. A back-to-back convertor comprising the generator side convertor and the grid-side convertor connects the synchronous generator to the grid. Back-to-back converters are connected to the PMSG generator terminals and the PMSG grid controller to optimize collected energy at the generator side at different wind speeds [14]. The converters control and distribute active and reactive power to the grid by maintaining a steady DC-Link voltage at the inverter input. Several converter designs for wind turbine applications are suggested in literature [15] such as the vector-controlled Back-to-Back converters based on the traditional PID controller. 3-phase inverters specifically use vector control. Uehara *et al.,*[16] describes a method for smoothing the output power of a PMSG based WECS by controlling the DC-link voltage and pitch angle. The construction of the WTE maximum power extraction and feeding of generated power to the grid. According to Khattak *et al.,* [17], several factors influence the performance and efficiency of turbines such as turbine component, wind speed, materials used etc. As the wind speed decrease, the power generated from wind turbines decreases proportionally [39].

Laghridat *et al.,* [18] introduced Comparative analysis between PI and linear-ADRC control of a grid connected variable speed wind energy conversion system (WECS) based on a squirrel cage induction generator. The system has high kernel ESO function for inaccurate system model, which facilitates estimation of total disturbances. Mastanamma and Subbarayudu [19] represents a Sliding Mode Control (SMC) Design for Variable Speed Wind Farm Systems (VS-WFS), which depends on and connected to an electrical network utilizing the Permanent Magnet Sync Generator (PMSG)). By utilizing Variable control has acquired that it is not difficult to utilize existing electronics for the variable speed wind energy converter control. The drawback is the increase in mechanical stress because of the squawking, which can diminish utilizing various techniques. The overall performance evaluation of PMSG can be expanded using advanced optimization methods by a number of control systems. to enhance the performance measurement of PMSG. The simulation results obtained show that the system has low efficiency. Tan *et al.,* represented a typical WECS structure consists of a rectifier on the PMSG side and a dc-link-system on the grid side inverter [20]. The rectifier controls of the PMSG's power or speed. The detachment of the condenser empowers totally separate control of each power electronic system. The inverter synchronizes the WECS power with the grid and keeps the DC voltage constant.

Yang *et al.,* [21] modeled and simulated a variable-speed wind turbine along with a PMSG. Despite the variable wind speed from 12 to 15 m/s, the difference in rotor speed was negligible [22]. They examined a Permanent Magnet Synchronous Generator (PMSG) gearless variable speed wind turbine device. By using MATLAB / Simulink, a gearless variable speed wind turbine scheme with PMSG was implemented.

Baran and Jąderko *et al.,* [23] conducted a simulation study on a variable structure control method for a small fixed-pitch variable-speed WECS based on a three-phase PMSG operating in variable wind environment. The WECS is connected to the grid via two back-to-back voltage source

converters (VSCs) via a direct current link. The control technique provided here is based on feedforward adjustment of the wind turbine's aerodynamic torque as assessed by a linear disturbance observer (DOB). Even though the authors obtained good results, the presented results are not verified and validated. Elbeji *et al.,* [24] proposed a PMSG based model and control techniques for a variable speed wind turbine. The model depicts the wind turbine's aerodynamics, mechanics, and electrical components. However, the system has drawbacks such as the performance of the WECS is determined by the pitch angle and the aerodynamic power is affected by wind speed. In addition, simulation results indicate that the system does not attain maximum values for the coefficient power, turbine power and speed ratio is not optimal.

A unified power control technique is presented by Geng *et al.,* [25] for WECS-based on PMSGs operating under different grid conditions. The generator-side converter is used to control the dc-link voltage, whereas the grid-side converter is used to control the injected power into the grid. The generator-side controller is designed to dampen torsional oscillations produced by drive-train characteristics and incorporates an additional damping loop. The effectiveness of the suggested system was validated using simulations. Based on the simulation results, the key limitation of the system is insufficient oscillation.

3. Methodology

In this study, a wind turbine model is simulated using MATLAB/SIMULINK. The turbine performance coefficient is determined by the turbine's mechanical output power based on the following: wind power and wind speed, rotary speed, and pitch angle function. An ADRC controller which relies on ESO function for estimating internal and external disturbances is adopted. The estimated disturbances are actively rejected without loading the controller. Thus, the main function of the controller remains that of tracking the references and system dynamics.

3.1 Design of Wind Turbine, Gear Ratio and PMSG

Wind power is given by [21]

$$P_w = \frac{1}{2}\rho A v_w^3 \tag{1}$$

While the power captured by a wind turbine is given by

$$P_{WT} = \frac{1}{2}c_P(\lambda,\beta)\rho A v_w^3 \tag{2}$$

The parameter $c_P(\lambda,\beta)$ is the power coefficient, which is the function of tip-speed ratio (TSR, denoted by λ) and the pitch angle β[26]. The nominal speed of the wind in the region of system installation is 4.3m/s [27]. Since the wind-speed is very low, a large wind turbine will be required. The turbine will require considerable height. The wind speed at a given height [28] is given by

$$v_w = v_0\left(\frac{H}{H_0}\right)^{\alpha} \tag{3}$$

Combining (1) and (3) and assuming $H = D$, where D is the diameter of the turbine, with $A = \frac{\pi}{4}D^2$, the wind power is

$$P_w = \frac{\pi}{8H_0^{3\alpha}} \rho v_0^3 D^{(2+3\alpha)} \tag{4}$$

With $H_0 = 10m$, $\alpha = 0.245$ and $P_w = 2 \times 10^6$W and assuming 50% efficiency, the value of diameter is computed to be approximately 175 m ($R = 87.5$m). However, this diameter is smaller than that of the Halide-X, which measures 220 m making it the most powerful offshore wind turbine built in the world today [29]. The power coefficient [30] $c_P(\lambda, \beta)$ is defined as

$$c_P(\lambda, \beta) = c_1 \left[\frac{c_2}{\lambda_i} - c_3\beta - c_4\right] \exp\left(-\frac{c_5}{\lambda_i}\right) \quad + c_6\lambda \tag{5}$$

where the parameter λ_i is defined as

$$\frac{1}{\lambda_i} = \frac{1}{\lambda + 0.08\beta} - \frac{0.035}{\beta^3 + 1} \tag{6}$$

Using the definition of $c_P$above, it is found that TSR will be 8.11. But for actual implementations, this value is quite low. For an n-blade machine, turbine's optimal rotational speed is defined as

$$\omega_{opt} = \frac{2\pi V}{n\left(\frac{R}{2}\right)} = \frac{4\pi v_w}{nR} \tag{7}$$

Using the available data ($n = 3$), $\omega_{opt} = 0.2058$ rads^{-1}. Thus, optimal TSR will be

$$\lambda_{opt} = \frac{\omega_{opt} R}{v_w} = 4.2$$

As the rotational speed is quite low, it should be increased. Assuming a gear ratio of 25, the input speed to the shaft of the generator will become 5.145 rads^{-1}. The permanent magnet synchronous generator (PMSG) is the synchronous generator by design, the relationship between rotational speed and the steady-state RMS back-EMF is defined as $V_{GEN} = K_v \omega_{\text{in}}$. An RMS voltage of 600V is required, therefore, $K_v = V_{GEN}/\omega_{\text{in}} = 107.8167\text{V}\ (\text{rads}^{-1})^{-1}$. Such a large value of voltage-constant can be realized by having large number of poles. This completes design of the components before the converters.

3.2 Design of Boost Converter

When the converter is operated under continuous-conduction mode, the value of peak-to-peak rippled inductor current is found to be

$$\Delta i_L = \frac{DV_{\text{in}}}{fL} \tag{8}$$

This relationship can be used to compute the required value of inductor. The value of ripple voltage across the capacitor is defined as

$$\Delta v_C = \frac{DI_O}{fC} \tag{8}$$

While the average input and output voltages are defined as

$$V_O = \frac{1}{1-D} V_{\text{in}} \tag{9}$$

With input and out voltage specifications given in Table 1, the duty cycle D is found to be $D = 0.25$. The boost converter parameters in Table 1 were calculated by using Eq. (8) – (10).

Table 1
Boost Converter Parameter

Parameter	Value	Parameter	Value
V_{in}	600V	V_O	800V
D	0.25	f_{SW}	3000 Hz
ΔI_L	25A	ΔV_C	0.8V
C	0.0781 F	ΔV_C	100μH

3.3 Active Disturbance Rejection Control (ADRC) and Its Design

Any physical system could be non-linear up-to some extent. Such a system can be described as

$$y^{(n)} + f(t) = b_0 u \tag{10}$$

Assuming $n = 2$, a state-variable implementation of the system can be written as

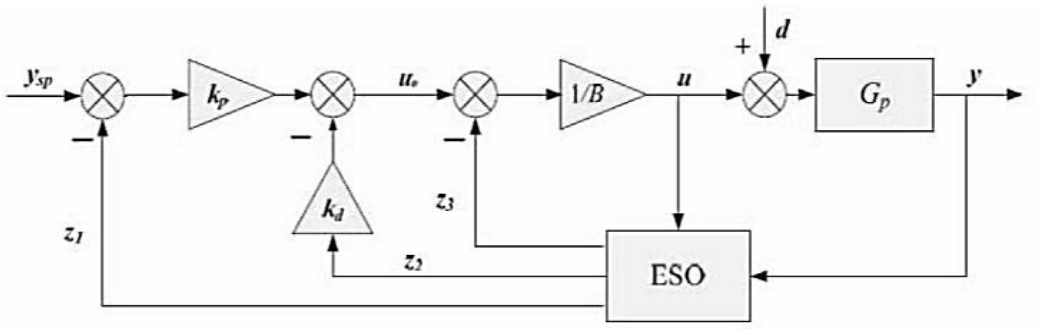

Fig. 3. Block Diagram of ADRC

$$\begin{bmatrix} \dot{x}_1 \\ \dot{x}_2 \\ \dot{x}_3 \end{bmatrix} = \begin{bmatrix} 0 & 1 & 0 \\ 0 & 0 & 1 \\ 0 & 0 & 0 \end{bmatrix} \begin{bmatrix} x_1 \\ x_2 \\ x_3 \end{bmatrix} + \begin{bmatrix} 0 \\ b_0 \\ 0 \end{bmatrix} + \begin{bmatrix} 0 \\ 0 \\ 1 \end{bmatrix} \dot{f}(t) \tag{11}$$

It should be noted that the 3rd state x_3 represents unknown disturbances/noises contained in $f(t)$. ADRC is all about actively rejecting $f(t)$ given that $x_3 \cong f(t)$. It should also be noted that x_3 is an extra-state, which must be estimated for the proper implementation of ADRC. The job of state estimation including the extra state is accomplished by extended-state observer (ESO). The dynamics of the observer are described as

$$\begin{bmatrix} \dot{\hat{x}}_1 \\ \dot{\hat{x}}_2 \\ \dot{\hat{x}}_3 \end{bmatrix} = \begin{bmatrix} 0 & 1 & 0 \\ 0 & 0 & 1 \\ 0 & 0 & 0 \end{bmatrix} \begin{bmatrix} x_1 \\ x_2 \\ x_3 \end{bmatrix} + \begin{bmatrix} 0 \\ b_0 \\ 0 \end{bmatrix} u + \begin{bmatrix} l_1 \\ l_2 \\ l_3 \end{bmatrix} (y - \hat{x}_1) \tag{13}$$

After some simplifications,

$$\begin{bmatrix}\dot{\hat{x}}_1\\ \dot{\hat{x}}_2\\ \dot{\hat{x}}_3\end{bmatrix}=\begin{bmatrix}-l_1 & 1 & 0\\ -l_2 & 0 & 1\\ -l_3 & 0 & 0\end{bmatrix}\begin{bmatrix}x_1\\ x_2\\ x_3\end{bmatrix}+\begin{bmatrix}0\\ b_0\\ 0\end{bmatrix}+\begin{bmatrix}l_1\\ l_2\\ l_3\end{bmatrix}y \tag{12}$$

The Eq. (12) can be used to design the observe parameters. while defining a control law

$$u=\frac{1}{b_0}\left[k_p(r-x_1)-k_i x_2+f(t)\right] \tag{15}$$

And by inserting in Eq. (10)

$$y''+k_i y'+k_p y=k_p r \tag{13}$$

The expression (13) can be used to obtain the ADRC parameters. Parameters of both ADRC, k_p and k_i and of ESO, l_1, l_2 and l_3 can be computed using arbitrary pole-placement theory [31] (feedback control design in state-space). The power of the ADRC control will force the process/plant to track desired control command. The transfer function of the boost converter is defined as

$$\frac{V_O(s)}{d(s)}=\frac{-\frac{V_O}{(1-D)RC}\left(s-\frac{R(1-D)}{L}\right)}{s^2+\frac{1}{RC}s+\frac{(1-D)^2}{LC}} \tag{14}$$

From the definition of ADRC's required differential equation, as in (10), from (14)

$$v_o''+f(t)=\frac{V_O}{LC}\,u \tag{15}$$

It should be noted we only need the values of average output voltage, the filtering parameters L and C for the design of ADRC control system. For a percentage overshoot of less than 5% and a settling time of 2ms, the damping ratio of the closed loop system will be 0.69, and the undamped natural frequency (using 2% settling-time criteria [32], $t_s=4/\zeta\omega_n$) of 2898.6 rad/s. Thus, the dominant pair of poles will be

$$s_{1,2}=-\zeta\omega_n\pm j\omega_n\sqrt{1-\zeta^2}=-2000\pm j2098$$

Now, the characteristic equation of the desired system will become $s^2-(s_1+s_2)s+\left(\mathrm{Re}^2(s_{1,2})+\mathrm{Im}^2(s_{1,2})\right)=s^2+4000s+8401604=0$. Comparing this equation with Eq. (13), the ADRC parameters and the observer parameters are found to be $k_p=8.402\times10^6$, $k_i=4000$. The ESO poles should further be pushed into negative complex plane, toward negative infinity. This will make quick estimation of required states. A simple criterion for the location of ESO poles is $s_{1,2,3}=(2\sim10)\times\mathrm{Re}(s_{1,2}^{ADRC})$. It should be noted all ESO poles will be placed on negative real axis, to make the ESO response overdamped. Underdamped ESO can produce undesired overshoot in the estimated states. Overdamped ESO will give no overshoots in estimated states. In this work, $S^{ESO}=4\times\mathrm{Re}(s_{1,2}^{ADRC})=8\times10^3$. The desired characteristic equation of the ESO becomes $s^3+2.4\times10^4s^2+1.92\times10^8s+5.12\times10^{11}$. Thus, ESO parameters are found to be $l_1=2.4\times10^4$, $l_2=1.92\times10^8$ and $l_3=5.12\times10^{11}$. The wind turbine model is presented next.

3.4 Inverter Modeling & Control

The function of the grid-side converter is to transfer the energy from the PMSG side to the electrical utility grid, control the DC-interface voltage and to accomplish power factor closer to one [33]. Therefore, Direct Power Control (DPC) is used to control the random input power. Although, the DC voltage from the generator-side converter is regulated, the power is not constant.

3.5 The PMSG-Based Wind Turbine System

A PMSG-based system has the ability to work over a wide range of wind speed. According to the intensity of the wind, the wind turbine generator needs to be controlled to operate in three different modes, as shown in Figure 4.

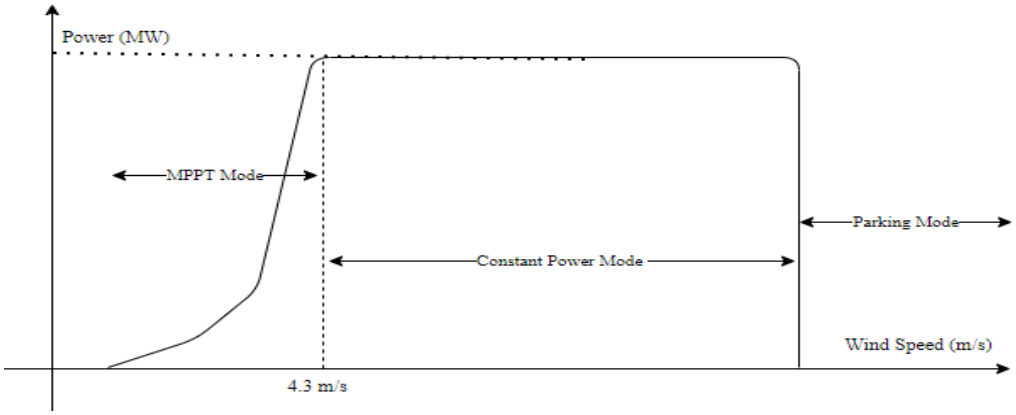

Fig. 4. Wind-Turbine Power Characteristics

To maximize power extraction, the control operation takes one of three modes: parking mode, MPPT mode and the constant power mode. If the wind speed is lower than cut-in speed, there is no power to rotate the turbine. If the wind speed is higher than safe operating speed, the turbine is forced to stop operating, and this is called parking mode. If the wind blows in range from cut-in speed to nominal speed, the system is in MPPT mode. As the speed increases beyond nominal speed, pitch control sets the pitch directions for the blades such that generated power does not damage the system. In this design, the pitch controller is based on PI control. The average wind speed considered is 2.8 m/s, with a minimum speed of 0.9 m/s and a maximum speed of 6.3- meter-per-second. There are seldom wind gusts, about 2 to 3 times a year. Around 90% of the useful wind distribution are between 0.9 m/s to 6.3 m/s therefore the turbine will have to be operated in MPPT mode [34]. Also, since the wind speed is quite low as compared with the minimum wind-speed required for most commercial WEC systems, a specifically designed turbine would be required. The rotor diameter of the turbine can exceed 200 meters so it will have to be installed at considerable height. The MPPT curve for the turbine is shown in Figure 5.

As shown in Figure 6, maximum power extraction happens at the optimal TSR, where the contrast between the actual TSR (blue curve) and the line characterized by a constant TSR is the lowest. This difference addresses the power in the wind that is not captured by the wind turbine. Frictional losses, limited wing size, and turbine design losses represent part of the uncaptured wind power and are enhanced by the fact that a wind turbine does not work at the optimal TSR across its operating range of wind speeds.

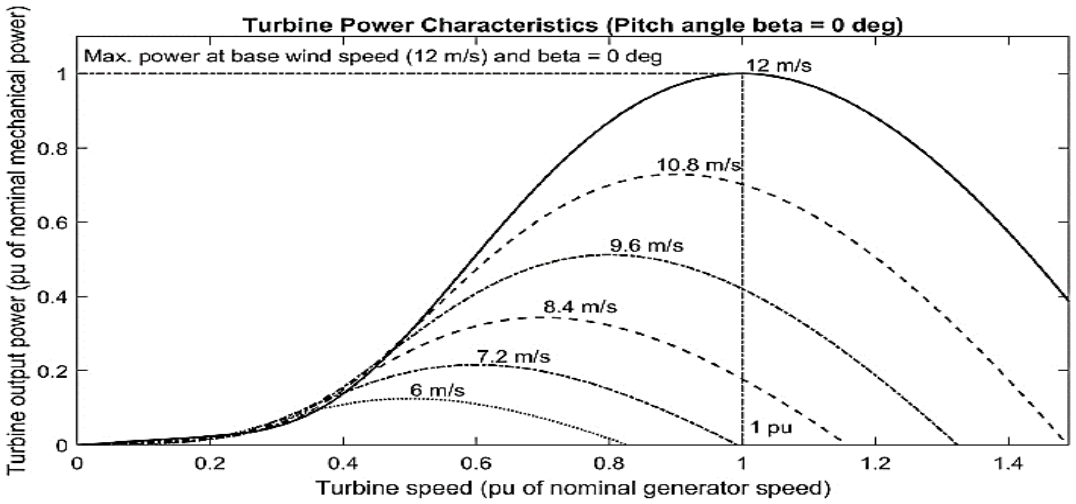

Fig. 5. Turbine Power Characteristic with Maximum Power Point Tracking

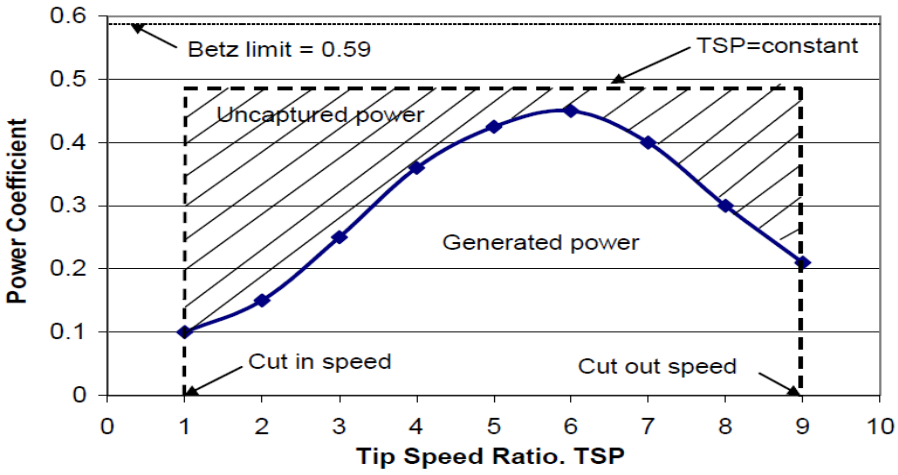

Fig. 6. Power Coefficient as the Function of TSR

3.5.1 Optimal Tip Speed Ratio

For a wind turbine with 3 blades, it has been empirically observed that $\lambda_{opt} \approx 5.24 - 5.45$. The design in this paper has achieved a value of 4.2 (see calculations following equation (7)). From the wind turbine's model, $C_{Pmx} = 0.48$, $\lambda_{opt} = 4.2$, and $R = 87.5m$. Figure 6 describe the Betz, ideal constant, and actual wind turbine power coefficient as a function of the TSR. Given all the values, the reference value of the turbine's rotational speed (run-time) is given by

$$\omega_{ref} = \frac{\lambda_{opt}}{R} v \tag{16}$$

3.5.2 The Power Output from The System

There are several constraints which affect the actual output power form the system. Firstly, the actual power is reduced by the number blades. It has been established by the designers; 3-blade turbines can capture the maximum wind power [34]. Betz's law has established an upper limit on the maximum power which can be captured in only 59%. The available power is also affected by the pitch angle. A mathematical description of the output power from the wind turbine is given by

$$P_{\text{out}} = \frac{1}{2} c_P(\lambda, \beta) \rho A v^3 \tag{17}$$

The parameter c_P is the coefficient of power, which is the function of TSR, λ, and the pitch angle β. The parameter ρ is the density of air, and A is the cross-sectional area swept by the turbine's blades.

4. Simulation Results and Discussion

Figure 7 shows the implementation of the PMSG WECS with ADRC Controller in Simulink. This model is validated by simulation results presented by Laghridat *et al.,* [18]. The model achieved 98 % efficiency, about 10 % improvement compared to that presented by Laghridat *et al.,* which achieved an efficiency of 88 %. For the system design and simulation model, all system blocks are cascaded. The modeling and simulation of the PMSG wind energy conversion system with active disturbance rejection control is carried out in this paper. Obtained results indicate system robustness, high performance, good regulation and stability against internal and external disturbances compared to the system in [18], which has high kernel ESO function suggesting inaccurate system model and which makes it difficult to estimate the total disturbances. Obtained results also show improvement in the controller performance, which is validated by constant DC voltage at the interface of the generator-side and grid-side converters and achieves maximum power compared to the controller presented in [24]. The overall performance evaluation of PMSG could be improved by studying the maximum power point tracking (MPPT) and the repeated chain of energy conversion controlling the pitch angle for improving PMSG. Performance. Obtained simulation results indicate high efficiency, lower power coefficient and lower turbine power with a speed ratio below optimum. Performance results for our PMSG simulation model were compared to the performance measurement of the PMSG in [19], which is based on the sliding mode control (SMC) system design for variable speed wind systems. This approach which can be augmented by advanced optimization techniques with several control mechanisms to enhance the performance. Furthermore, results for the proposed system indicate high system efficiency.

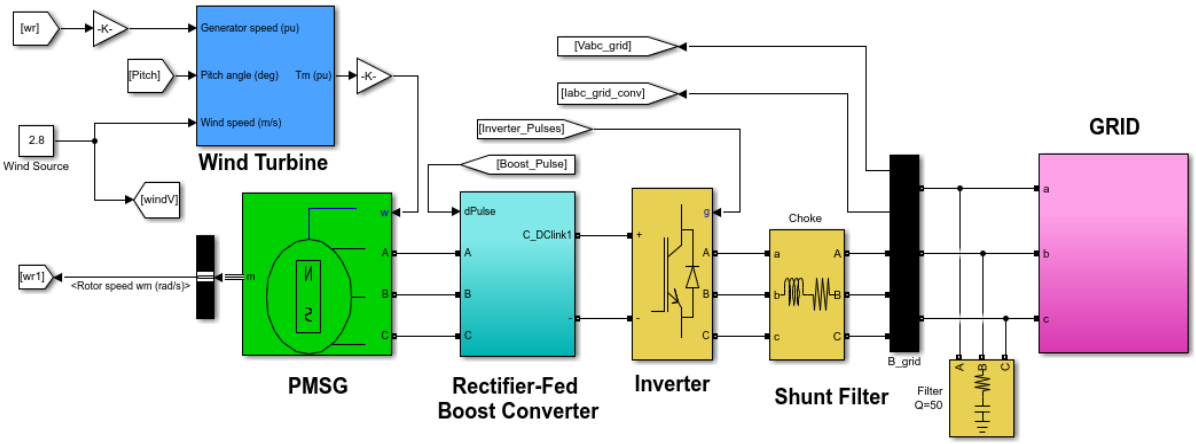

Fig. 7. System Implementation

4.1 Wind-Turbine Settings

The base power of the turbine is set at 2MW, with base wind velocity of 4.3m/s. Since the wind speed is quite low, assuming 50% turbines efficiency, turbine diameter is 175m. It should be noted

that turbines rotational speed will be quite low. Using Eq. (16), this is found to be 0.2226 rad/s. Although rotational speed is quite low, this may not be able to rotate the most commercial turbines. But, with efficient blade design, power can be extracted from low-speed winds [35]. The reference power of the wind-turbine at a particular speed is computed using the curve shown in Figure 4.

4.2 PMSG

Suitable rotational speed is applied to the shaft of the PMSG generator. The rotational speed was calculated and given as 5.565rad/s. Such a low speed requires a generator with huge number of pole pairs. The number of poles pairs are found to be 24 for 50Hz output voltage/power.

4.3 Boost Converter Controller

Design of the boost converter and controller thereof is described above and the block diagram representation for the controller implementation is shown in Figure 8. The Simulink implementation of the controller can be understood by looking at Figure 3. On the other hand, implementation of the inverter controller is accomplished using the conventional method described in [36,37]. Figure 9 shows the comparison of the system real power versus apparent power. The real power increases steadily after start-up between 0.03 s and 0.5 s, then stabilises. While the apparent power remains zero after start-up.

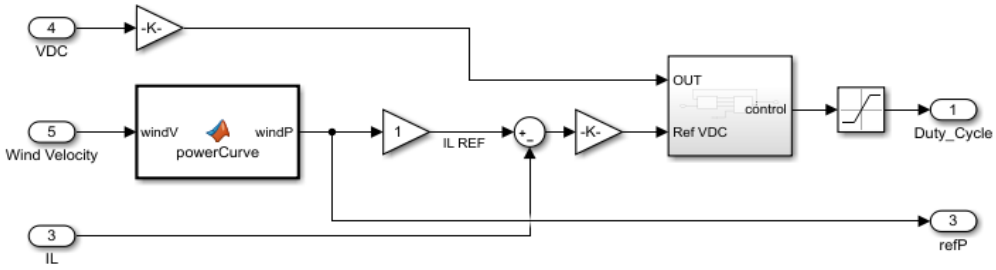

Fig. 8. Computation of Reference Power

4.4 Simulation Results

The simulation results were obtained by running the MATLAB/Simulink model for various lengths of times. The simulation graphs show the dynamic response of the system and indicate that the system reached steady state within the 0.05 seconds of simulation runtime. Figure 9 – Figure 15 display graphs for the simulation results. The comparison of the system real power versus active power are shown in Figure 9, while the output voltage of the boost converter and shaft speed of the PMSG are shown in Figure 10. Figure 11 shows the voltage and current delivered to the grid by the inverter, with all values shown in pu. Figure 12 shows the voltage and current of the load. To compare the performance of the ADRC controller with the performance of the conventional PI controller, the ADRC controller is replaced with PI controller and the results for the active and reactive power of the system and output voltage of the boost converter are shown in Figure 13 and in Figure 14 respectively. Finally, Figure 15 shows the voltage and current of the system with the PI controller for same loading as with the ADRC controlled system.

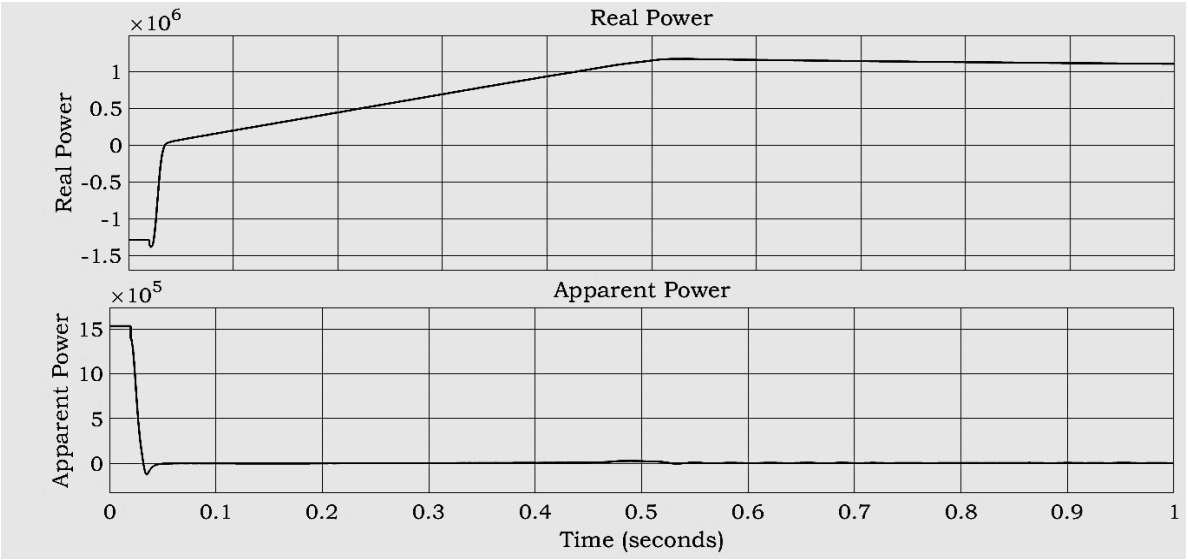

Fig. 9. Comparison of System Real Output Power Versus Apparent Output Power with ADRC controller

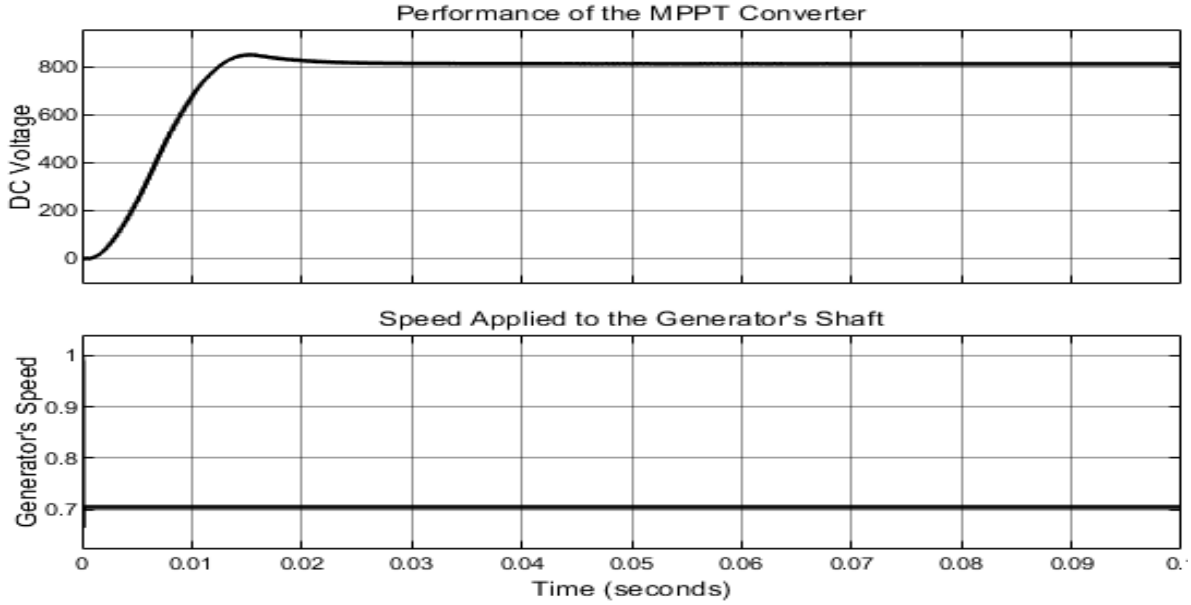

Fig. 10. DC Output Voltage of Boost Converter and shaft speed of the PMSG WECS with ADRC controller

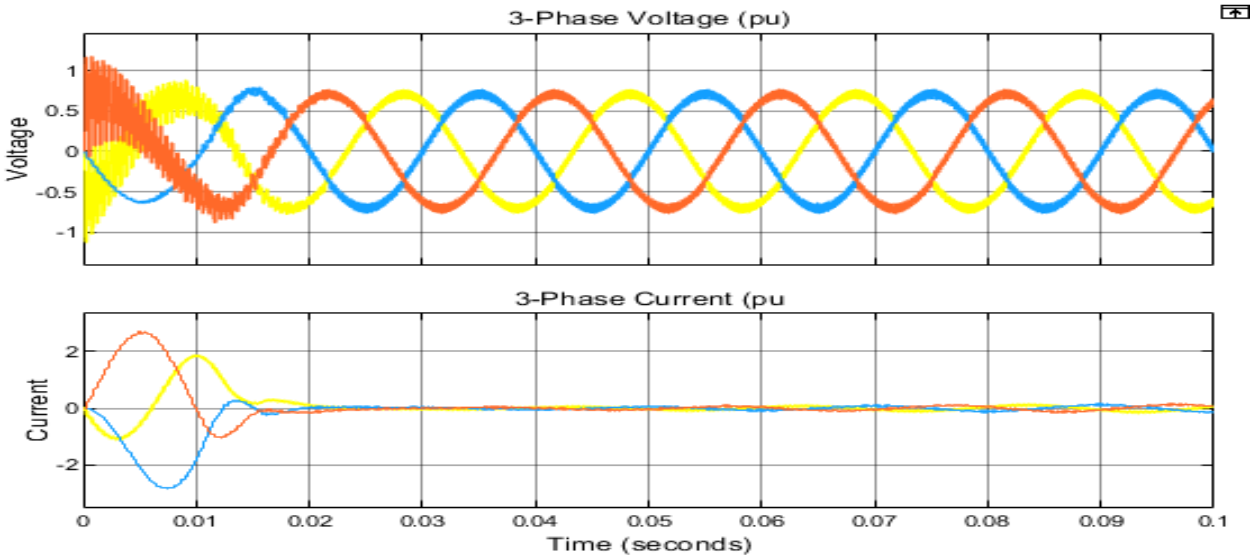

Fig. 11. Inverter 3-Phase Voltage and Current (pu) delivered to the grid

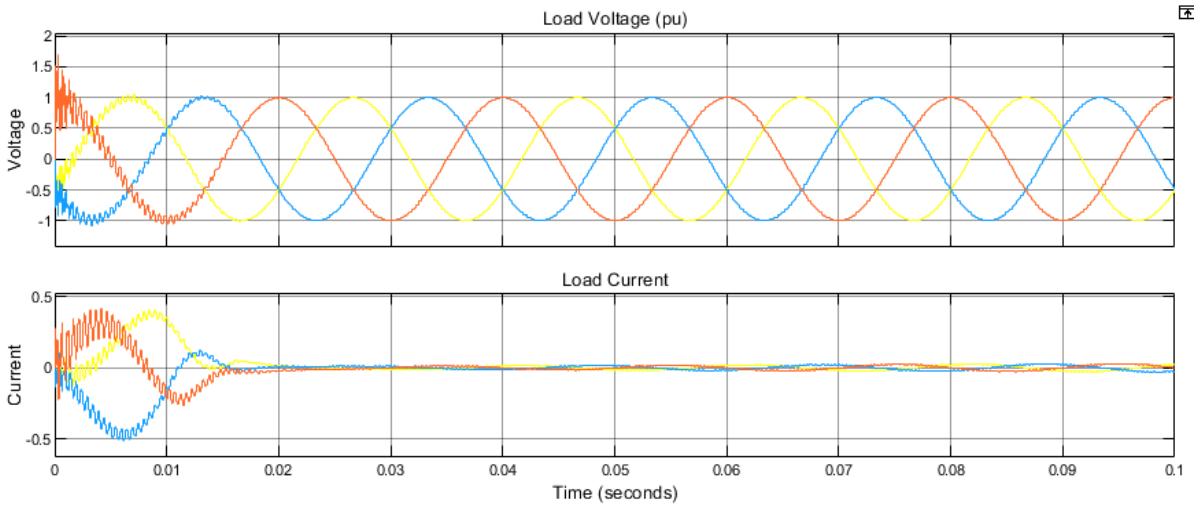

Fig. 12. Load Voltage and Current (pu) of the system with ADRC controller

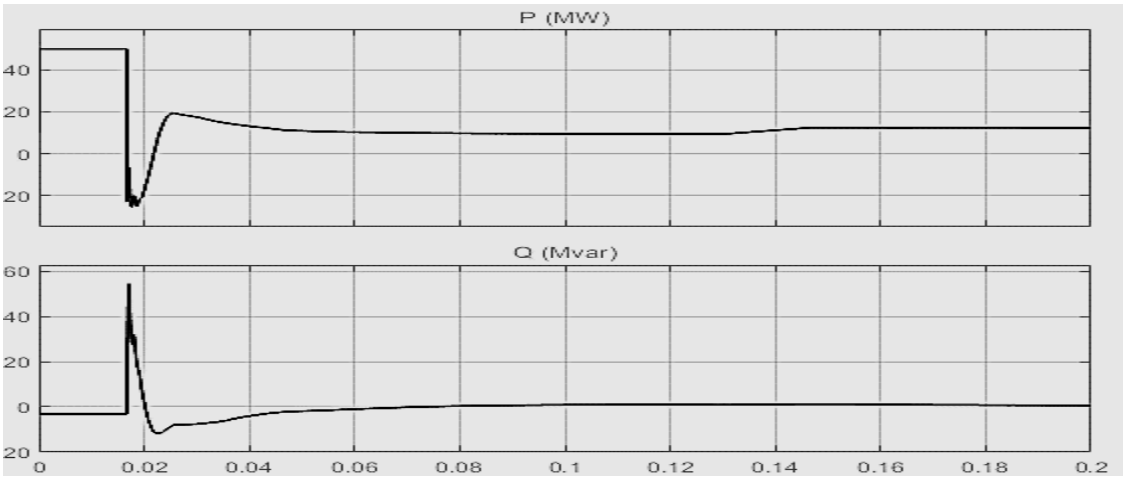

Fig. 13. Comparison of the System Real Output Power Versus Reactive Output Power with PI Controller

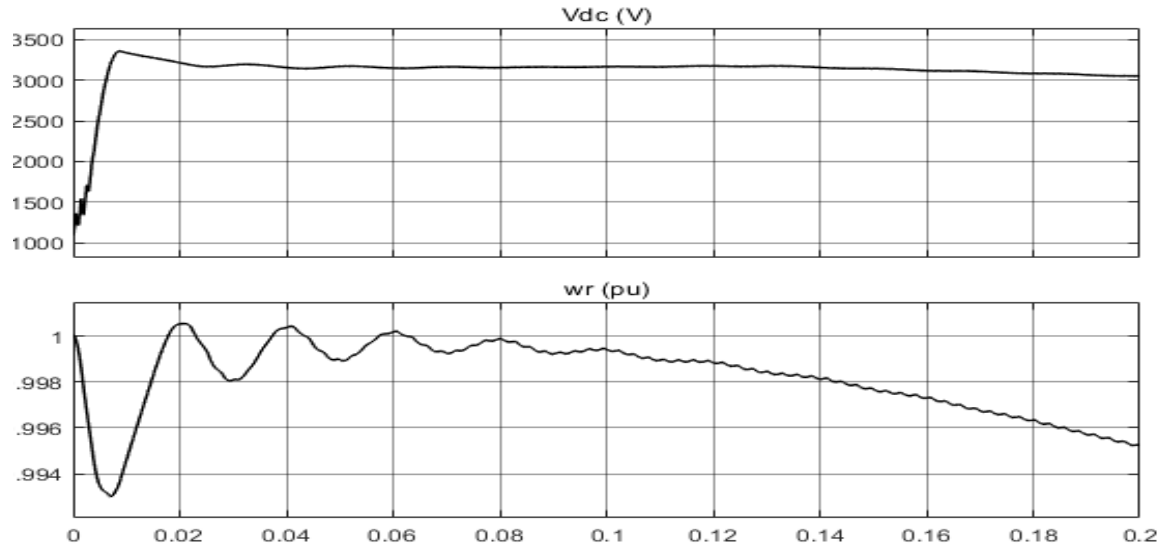

Fig. 14. DC Voltage Output Voltage of Boost Converter and Shaft Speed of PMSG WECS with PI Controller

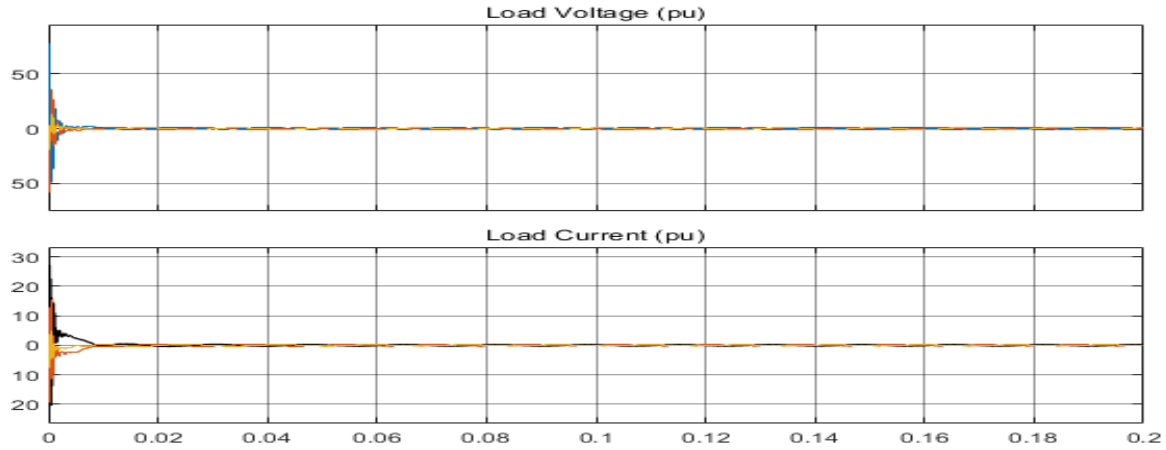

Fig. 15. Load Voltage and Current (pu) of the system with PI controller

4.5 Results and Discussion

The results of the proposed system are described and analyzed as follows. Firstly, the performance results for the ADRC controlled system are presented, followed by the performance results for the PI-controlled system. The power stability performance of the system can be seen in Figure 9 as illustrated by the comparison of the system real output power versus reactive output power. The power stability performance refers to attaining constant steady power with variable speed input. The simulation is run for constant input nominal speed of 4 m/s from 0 s to 1 s, then a disturbance is introduced at 1 s by decreasing the wind speed from nominal 4 m/s to 3 m/s from 1 s to 2 s. The system is designed to produce 2MW at this speed. The results in Figure 9 indicate stable generation of required power. According to the Betz's law, maximum energy production could be up-to 1.186MW. The simulated designed system is producing an output power of 1.17MW (from Figure 9). This indicates that the system efficiency is 98.65%. The performance of the MPPT controller can be observed from Figure 10 through Figure 12. The MPPT control is not only providing constant voltage with varying wind speed, but it is also tracking the available power successfully. The set-point voltage for the controller was set to 800V. Thus, even in the presence of loading, the ADRC controller has successfully tracked the available power while regulating the DC voltage. The control of the inverter is implemented independent of the MPPT controller. An LC shunt filter links the inverter

output to the load. The LC filter filters the inverter output voltage and current providing a smooth voltage and current for the load. Figures 11 and 12 show the unfiltered inverter voltage and current versus the filtered inverter voltage and current at the load. As shown by the results, the LC filter successfully smoothened the inverter output voltage and current and frequency stability was achieved. The PI controller was applied to the proposed system for comparison only in term to prove the effectiveness of the proposed control approach. The results from PI-controlled system are shown in Figure 13 (output power regulation and rejection of Q-power) and results with ADRC are shown in Figure 9, Figure 14 shows results of DC voltage regulation from the boost convertor with PI controller and Figure 10 shows results for ADRC controller and Figure 15 shows the load and current of the system with PI controller. As a comparison, the performance of ADRC controlled system out-performs as opposed to PI controlled system. Firstly, the power stability is very poor compared with ADRC's performance shown in Figure 9. Although transients are slower in the case of ADRC, but the transitions are smooth, approaching ultimately to the desired power. PI controlled system's generation of sinusoidal power has almost been drastic. Particularly, the starting dynamics are unacceptable. While in the ADRC control, although there are initial dynamics, but are much better as compared to PI's performance. Finally, load regulation of the PI controlled system shown in Figure 15 indicates the superiority of the ADRC control as shown in Figure 11 and in Figure 12.

5. Conclusions

A PMSG Wind Energy Conversion System Using Active Disturbance Rejection Control was simulated. According as the Betz's law, maximum energy production is 1.186MW. The simulated designed system is producing an output power of 1.17MW. The system has excellent efficiency in terms of stability, precision and robustness against internal disturbances with an overall system efficiency of 98.65%. For future work, there are blocks such as the turbine model with its wind profile where the need of a controller cannot be ignored, pitch control, MPPT control using boost converter and the inverter switching control.

Additionally, a high-performance design of servo-based pitch control can be considered. Also, the world's research is constantly heading towards the development and installation of large-size wind turbine. The larger wind turbines can pose challenges to the safety of maintenance workers. So, the research should also consider the development of small and safe wind systems.

Acknowledgement
This research was not funded by any grant.

References

[1] Zuan, A. M. S., M. K. Z. Anuar, S. Syahrullail, M. N. Musa, and E. A. Rahim. "A study of float wave energy converter (FWEC) model." *Journal of Advanced Research in Applied Sciences and Engineering Technology* 1, no. 1 (2015): 40-49.

[2] Renewable Energy and Electricity | Sustainable Energy | Renewable Energy - World Nuclear Association. Accessed December 30, 2021. https://world-nuclear.org/information-library/energy-and-the-environment/renewable-energy-and-electricity.aspx.

[3] Jain, Bhavna, Shailendra Jain, and R. K. Nema. "Control strategies of grid interfaced wind energy conversion system: An overview." *Renewable and Sustainable Energy Reviews* 47 (2015): 983-996. https://doi.org/10.1016/j.rser.2015.03.063

[4] Gidwani, Lata. "A comparative power quality study of DFIG and PMSG based wind energy conversion system." *WSEAS transactions on systems and control* 10 (2015): 38-47.

[5] Jamil, Emad, Salman Hameed, and Basharat Jamil. "Power quality improvement of distribution system with photovoltaic and permanent magnet synchronous generator based renewable energy farm using static

synchronous compensator." *Sustainable Energy Technologies and Assessments* 35 (2019): 98-116. https://doi.org/10.1016/j.seta.2019.06.006

[6] Pichitkul, Auraluck, and Lakshmi N. Sankar. "Aerodynamic design and modeling of large-scale offshore wind turbines." *CFD Letters* 11, no.10 (2021): 1–14. https://doi.org/10.2514/6.2021-0814

[7] "Malaysia." Asia Wind Energy Association 2021. Accessed December 30, 2021. https://www.asiawind.org/research-data/market-overview/malaysia/.

[8] Ma, Ke. *Power electronics for the next generation wind turbine system*. Springer International Publishing, 2015. https://doi.org/10.1007/978-3-319-21248-7

[9] Han, Jingqing. "From PID to active disturbance rejection control." *IEEE transactions on Industrial Electronics* 56, no. 3 (2009): 900-906. https://doi.org/10.1109/TIE.2008.2011621

[10] Herbst, Gernot. "A simulative study on active disturbance rejection control (ADRC) as a control tool for practitioners." *Electronics* 2, no. 3 (2013): 246-279. https://doi.org/10.3390/electronics2030246

[11] Yu, Dachuan, Mahesh Sitaram Illindala, and Osama Mohammad Alkhouli. "Power inverter control for grid-tie transition." U.S. Patent 8,068,352, issued November 29, 2011.

[12] Huang, Yi, and Wenchao Xue. "Active disturbance rejection control: methodology and theoretical analysis." *ISA transactions* 53, no. 4 (2014): 963-976. https://doi.org/10.1016/j.isatra.2014.03.003

[13] Elnaggar, A.K., Rueda, J.L. and Erlich, I., Comparison of short-circuit current contribution of Doubly-Fed induction generator based wind turbines and synchronous generator. In *2013 IEEE Grenoble Conference*. https://doi.org/10.1109/PTC.2013.6652307

[14] Li, Shuhui, Timothy A. Haskew, Yang-Ki Hong, and Ling Xu. "Direct-current vector control of three-phase grid-connected rectifier–inverter." *Electric Power Systems Research* 81, no. 2 (2011): 357-366. https://doi.org/10.1016/j.epsr.2010.09.011

[15] Omeje, Crescent Onyebuchi. "Power Loss Analysis Model of a DC-DC Buck-Boost Converter with an Interfaced Three Phase Inverter for Medium Voltage Application." *Journal of Asian Scientific Research* 9, no. 8 (2019): 100-115. https://doi.org/10.18488/journal.2.2019.98.100.115

[16] Uehara, Akie, Alok Pratap, Tomonori Goya, Tomonobu Senjyu, Atsushi Yona, Naomitsu Urasaki, and Toshihisa Funabashi. "A coordinated control method to smooth wind power fluctuations of a PMSG-based WECS." *IEEE Transactions on energy conversion* 26, no. 2 (2011): 550-558. https://doi.org/10.1109/TEC.2011.2107912

[17] Khattak, M. A., NS Mohd Ali, NH Zainal Abidin, N. S. Azhar, and M. H. Omar. "Common Type of Turbines in Power Plant: A Review." *Journal of Advanced Research in Applied Sciences and Engineering Technology* 3, no. 1 (2016): 77-100.

[18] Laghridat, Hammadi, Ahmed Essadki, and Tamou Nasser. "Comparative analysis between PI and linear-ADRC control of a grid connected variable speed wind energy conversion system based on a squirrel cage induction generator." *Mathematical Problems in Engineering* 2019 (2019). https://doi.org/10.1155/2019/8527183

[19] Mastanamma, Y., and D. Subbarayudu. "Permanent Magnet Synchronous Generator for Wind Energy Conversion Systems (WECS): A Review." *management* 17, no. 18: 19.

[20] Tan, K. T., B. Sivaneasan, X. Y. Peng, and P. L. So. "Control and operation of a DC grid-based wind power generation system in a microgrid." *IEEE Transactions on Energy Conversion* 31, no. 2 (2015): 496-505. https://doi.org/10.1109/TEC.2015.2497709

[21] Yang, Yun, Kwan-Tat Mok, Siew-Chong Tan, and S. Y. R. Hui. "Low-power wind energy conversion system with variable structure control for DC grids." In *2014 IEEE 5th International Symposium on Power Electronics for Distributed Generation Systems (PEDG)*, pp. 1-6. IEEE, 2014. https://doi.org/10.1109/PEDG.2014.6878655

[22] Fandi, Ghaeth, Famous O. Igbinovia, Ibrahim Ahmad, Jan Svec, and Zdenek Muller. "Modeling and simulation of a gearless variable speed wind turbine system with PMSG." In *2017 IEEE PES PowerAfrica*, pp. 59-64. IEEE, 2017. https://doi.org/10.1109/PowerAfrica.2017.7991200

[23] Baran, Janusz, and Andrzej Jąderko. "An MPPT control of a PMSG-based WECS with disturbance compensation and wind speed estimation." *Energies* 13, no. 23 (2020): 6344. https://doi.org/10.3390/en13236344

[24] Elbeji, Omessaad, Mouna Ben Hamed, and Lassaad Sbita. "PMSG wind energy conversion system: Modeling and control." *International Journal of Modern Nonlinear Theory and Application* 2014 (2014). https://doi.org/10.4236/ijmnta.2014.33011

[25] Geng, Hua, Geng Yang, Dewei Xu, and Bin Wu. "Unified power control for PMSG-based WECS operating under different grid conditions." *IEEE Transactions on Energy Conversion* 26, no. 3 (2011): 822-830. https://doi.org/10.1109/TEC.2011.2127478

[26] Chen, Zhe, Jianzhong Zhang, M. Cheng, and Xiaofan Fu. "Pitch Angle Control for Variable Speed Wind Turbines." In *Proceedings of the Third International Conference on Electric Utility Deregulation and Restructuring and Power Technologies (DRPT 2008)*. IEEE, 2008. https://doi.org/10.1109/DRPT.2008.4523867

[27] Ali Kadhem, Athraa, Noor Izzri Abdul Wahab, and Ahmed N Abdalla. "Wind energy generation assessment at specific sites in a Peninsula in Malaysia based on reliability indices." *Processes* 7, no. 7 (2019): 399. https://doi.org/10.3390/pr7070399
[28] Masters, Gilbert M. *Renewable and efficient electric power systems*. John Wiley & Sons, (2013): 410-498.
[29] "Haliade-X Offshore Wind Turbine." World's Most Powerful Offshore Wind Platform: Haliade-X | GE Renewable Energy. Accessed December 30, 2021. https://www.ge.com/renewableenergy/wind-energy/offshore-wind/haliade-x-offshore-turbine.
[30] Ragheb, Magdi, and Adam M. Ragheb. "Fundamental and Advanced Topics in Wind Power." *Fundamental and advanced topics in wind power* 1, no. 1 (2011).
[31] Moothedath, Shana, Prasanna Chaporkar, and Madhu N. Belur. "Minimum cost feedback selection for arbitrary pole placement in structured systems." *IEEE Transactions on Automatic Control* 63, no. 11 (2018): 3881-3888.
[32] Katsuhiko, Ogata. *Modern control engineering*. 2010. https://doi.org/10.1109/TAC.2018.2800787
[33] Errami, Y., Mohammed Ouassaid, and Mohamed Maaroufi. "Control of a PMSG based wind energy generation system for power maximization and grid fault conditions." *Energy Procedia* 42 (2013): 220-229. https://doi.org/10.1016/j.egypro.2013.11.022
[34] Thongam, Jogendra Singh, and Mohand Ouhrouche. "MPPT control methods in wind energy conversion systems." *Fundamental and advanced topics in wind power* 15 (2011): 339-360.
[35] Hameed, M. Saqib, and S. Kamran Afaq. "Design and analysis of a straight bladed vertical axis wind turbine blade using analytical and numerical techniques." *Ocean Engineering* 57 (2013): 248-255. https://doi.org/10.1016/j.oceaneng.2012.09.007
[36] Bao, Xianwen, Fang Zhuo, Yuan Tian, and Peixuan Tan. "Simplified feedback linearization control of three-phase photovoltaic inverter with an LCL filter." *IEEE Transactions on Power Electronics* 28, no. 6 (2012): 2739-2752. https://doi.org/10.1109/TPEL.2012.2225076
[37] Laaksonen, Hannu, Pekka Saari, and Risto Komulainen. "Voltage and frequency control of inverter based weak LV network microgrid." In *2005 International Conference on Future Power Systems* 5, no. 2 (2005). https://doi.org/10.1109/FPS.2005.204293